Vagal regulation of Group 3 innate lymphoid cells and the immunoresolvent PCTR1 controls infection resolution

Jesmond Dalli[1,2], Romain A. Colas[1,2], Hildur Arnardottir[1,†], and Charles N. Serhan[1]

[1]Center for Experimental Therapeutics and Reperfusion Injury,
Harvard Institutes of Medicine, Department of Anesthesiology, Perioperative and Pain Medicine, Brigham and Women's Hospital and
Harvard Medical School, Boston, USA MA 02115
[2] Lipid Mediator Unit, Biochemical Pharmacology, William Harvey Research Institute, Barts and the London School of Medicine, Queen Mary University of London, London, United Kingdom. EC1M 6BQ
[†]Present address: Department of Medicine, Solna (MedS), K2, Group G Hansson, Cmm, L8:03, Karolinska Universitetssjukhuset, Solna 171 76 Stockholm, Sweden
.

Contact:

Prof. Charles N Serhan, Harvard Institutes of Medicine, 77 Avenue Louis Pasteur, HIM 829, Boston, MA 02115. E-mail: cnserhan@zeus.bwh.harvard.edu;
Tel: 617-525-5001; Fax: 617-525-5017

Dr Jesmond Dalli, William Harvey Research Institute, John Vane Science Centre, Charterhouse Square, London. EC1M 6BQ. E-mail: j.dalli@qmul.ac.uk
Tel: +44 (0) 207 882 8263

Summary

Uncovering mechanisms that control immune responses in the resolution of bacterial infections is critical for the development of new therapeutic strategies that resolve infectious-inflammation without unwanted side effects. Herein, we found that disruption of the vagal system in mice delayed resolution of *Escherichia coli* infection. Dissection of the right vagus decreased peritoneal Group 3 innate lymphoid cell (ILC3) numbers and altered peritoneal macrophage responses. Vagotomy resulted in an inflammatory peritoneal lipid mediator profile characterized by reduced concentrations of resolvins, including the protective immunoresolvent PCTR1, along with elevated inflammation-initiating eicosanoids. We found that acetylcholine upregulated the PCTR biosynthetic pathway in ILC3s. Administration of PCTR1 or ILC3s to vagotomised mice restored tissue resolution tone and host responses to *E. coli* infections. Together these findings elucidate a host protective mechanism mediated by ILC3-derived pro-resolving circuit, including PCTR1, that is controlled by local neuronal output to regulate tissue resolution tone and myeloid cell responses.

eTOC

Resolution of the inflammatory response to infections is important for preventing damage to the host. Dalli et al. find that the vagus nerve promotes bacterial clearance by regulating tissue ILC3 numbers and upregulating the protective mediator PCTR1, which conditions peritoneal macrophage responses and promotes resolution of infection.

Introduction

Progression of the acute inflammatory response is highly coordinated, and when self-limited, leads to disposal of the inciting stimulus and re-establishment of function in affected organ(s) (Chiang et al., 2012; Fullerton et al., 2014; Leslie, 2015; Nathan, 2012; Serhan et al., 2015; Tabas and Glass, 2013; Ward, 2012). The initiation of this vital response is governed by diverse local signals that include cytokines, chemokines (Dinarello, 2011) and chemical mediators produced *via* stereospecific conversion of precursor essential fatty acids (Nakamura and Shimizu, 2011; Proia and Hla, 2015; Samuelsson, 2012; Serhan et al., 2015). These mediators form gradients that promote leukocyte recruitment to the site of injury and/or infection (Haeggstrom and Funk, 2011; Samuelsson, 2012). Termination or resolution of this host response is now appreciated to be an active process (Chiang et al., 2012; Leslie, 2015; Serhan et al., 2015) orchestrated by specific signals including gases (Flannigan et al., 2014), proteins (Leoni et al., 2015) as well as novel essential fatty acid-derived mediators (Leslie, 2015; Serhan et al., 2015; Tabas and Glass, 2013).

The first of the resolution phase lipid mediators described are now grouped in four new families of chemical mediators termed specialized pro-resolving mediators (SPMs) that include resolvins, protectins, lipoxins and maresins (Serhan et al., 2015). SPMs are each proven agonists in the host immune system regulating both innate (Campbell et al., 2010; Chiang et al., 2012) and adaptive immunity (Gao et al., 2015). These mediators display potent actions controlling phagocyte clearance of bacterial infections and reduce collateral tissue injury and inflammation. Consequently, dysregulated production of these pro-resolving mediators is associated with disease onset and/or severity (Chiang et al., 2012; Dalli et al., 2015b). Given the alarming increase in bacterial multidrug resistance there is an urgent need for the development of novel strategies to clear invading bacteria without compromising the host, as immune

suppresssion is a major side effect of many current therapeutics (Chiang et al., 2012; Nathan, 2012; Ward, 2012). Thus, understanding the endogenous mechanisms that regulate SPM production in infections can provide insights into potential novel therapeutic approaches for combatting infections that may limit unwanted side effects.

The neuronal reflex senses peripheral inflammation and coordinates the host response to injury and/or infection, regulating events within the initiation of inflammation (Pavlov and Tracey, 2012; Rosas-Ballina et al., 2011). Recently, we found that during acute sterile inflammation the vagal system regulates docosahexaenoic acid (DHA) derived pro-resolving mediators resolvin (Rv)D1, RvD3 and protectin D1(Mirakaj et al., 2014). In this context, the role of the neural reflex in regulating resolution status of peripheral tissues as well as the role(s) of this reflex in promoting the resolution of infectious-inflammation remains of interest. Thus it is critical to gain insights into these processes since they may facilitate development of host-directed resolution-based therapeutics to help combat infections (Lee and Zeldin, 2015). For this purpose, we investigated the impact of vagotomy on regulating the resolution mechanisms in the peritoneum as well as how this influenced innate immune responses during self-resolving *Escherichia coli* infections. Results from these experiments indicated that vagal disruption led to dysregulation of tissue retinoic acid–related orphan receptor γ t (RORγt)$^{+}$ CD335^{+} Group 3 innate lymphoid cell (ILC3) numbers, resting peritoneal lipid mediator profiles and macrophage responses. This in turn was associated with delayed resolution of infectious-inflammation. Together, the present findings identify ILC3 and PCTR1 as central mediators in neuronal control of host response to peritoneal infections.

Results

Vagotomy alters resting peritoneal lipid mediator profiles

Events occurring during the early phases of inflammation may have a profound impact on the amplitude and duration of these responses (Dalli et al., 2015a). SPMs orchestrate the host response to both sterile and infectious insults (Chiang et al., 2012; Dalli et al., 2015a). To establish the role of the vagus system in regulating the tissue pro-resolution tone we assessed peritoneal lipid mediator (LM) profiles prior to infectious challenge in sham and mice subjected to resection of the right vagus trunk. Using liquid chromatography tandem mass spectrometry (LC-MS-MS) based LM metabololipidomics we identified mediators from all three major bioactive metabolomes in peritoneal lavages (Figure 1a, b). These included the resolvins, protectins and maresins from docosahexaenoic acid, E-series resolvins and the arachidonic acid derived lipoxins, leukotrienes (LTs), thromboxanes (TXs) and prostaglandins (PGs). Multivariate analysis of lipid mediator profiles obtained from sham and vagotomised mice at 1, 3 and 7 days post-vagotomy showed that conditions segregated into distinct clusters (Figure 1c). Assessment of the loading plot for these lipid mediator profiles demonstrated a strong association between the recently elucidated host protective mediator PCTR1 (16R-glutathionyl, 17S-hydroxy-4Z,7Z,10Z,12E,14E,19Z-docosahexaenoic acid) (Dalli et al., 2015c) and sham mice with a Variable Importance in Projection (VIP; *see methods for details*) score >1. Moreover, the peritoneal PCTR1 concentration was reduced as early as 1 day after vagotomy, with the changes reaching statistical significance on days 3 and 7 when compared to peritoneal lavages from sham mice (Figure 1c and Table 1). In these lavages, there were also significant increases in the concentrations of several inflammation-initiating mediators such as $PGF_{2\alpha}$ compared to lavages from sham mice. These alterations in peritoneal lipid mediator profiles were

also associated with a time dependent decrease in peritoneal acetylcholine (ACh) concentrations following vagotomy (Figure 1d).

Peritoneal innate immunity is dysregulated in vagotomised mice

We next investigated whether vagotomy also led to perturbation of the resident peritoneal leukocyte population. In peritoneal lavages from naive mice we identified a cell population that was FSC^{low}, SSC^{low}, $Lineage^{-}$, $NK1.1^{low/-}$, $RoR\gamma t^{+}$, $CD127^{+}$, $CD117^{+}$, $IL23R^{+}$, $CD335^{+}$ that express a similar phenotypic profile to group 3 innate lymphoid cells (ILC-3) found in the intestinal lamina propria as well as those from spleens (Figure S1). To further characterize this novel ILC-3 population we sorted peritoneal ILC-3 using a validated gating strategy highlighted in Figure S2 that gave essentially identical cell numbers to that described in the literature (Robinette et al., 2015) and outlined in Figure S1. We then assessed the expression of a panel of genes that are upregulated in ILC-3 when compared to NK1.1 cells (Robinette et al., 2015). Realtime PCR analysis of these sorted cells demonstrated that peritoneal ILC-3 expressed higher levels of *Il-22, Il-23r, Il-1r1, Igfbp7* and *Pram1* (Figure S3) then NK1.1 cells. When next assessed the impact of vagotomy on these cells and found that when mice were subjected to vagotomy there was a perturbation of this cell population with a significant reduction in the number of these cells (Figure 2a). Disruption of the right vagus also led to a time dependent increase in the number of peritoneal $F4/80^{+}CD11b^{+}$ macrophages (Figure 2b). Vagotomy did not appear to substantially change either the $CD3^{+}$ T cells or $CD19^{+}B220^{+}$ B cells, whereas $NK1.1^{+}CD335^{+}$ natural killer (NK)-cell numbers (n=4 mice/group) were significantly reduced 1 day after vagotomy ($1.2\pm0.3 \times 10^{5}$ cells/mouse vs $5.8\pm0.5 \times 10^{5}$ cells/mouse in vagotomised vs sham mice) with their numbers recovering by day 3 and remaining stable through to day 7.

Vagotomy also led to time dependent alterations in the expression of macrophage phenotypic markers, including CD206 and major histocompatibility complex

class II (MHCII), when compared to cells from sham mice (Figure 2c and Table S1). Vagotomy also led to alterations in the lipid mediator profiles of peritoneal macrophages with a reduction in the concentrations of host protective mediators including PCTR1, PD1 and the lipoxin pathway marker 5,15-diHETE (Figure 2d, Table S2). Therefore these results demonstrate that disruption of the right vagus trunk leads to an alteration in the peritoneal leukocyte composition as well as macrophage phenotype.

Vagotomy of the right vagus trunk delays the resolution of infectious-inflammation

We next tested whether these perturbations in the tissue responses impacted the host's ability to clear bacterial infections. Inoculation of mice with 10^6 CFU *E. coli* resulted in a self-limited inflammatory response with maximal infiltration of $Ly6G^+CD11b^+$ neutrophils (Ψ_{max}) occurring at ~12h (T_{max}) followed by a decline (Figure 3a). Neutrophil numbers reached 50% of maximum (Ψ_{50}) at ~34h (T_{50}) giving a resolution interval (R_i), i.e. the difference between T_{max} and T_{50}, of ~22h. In contrast, in mice subjected to unilateral vagotomy of the right vagus *E. coli* inoculation led to a significant increase ($11.9\pm0.6 \times 10^6$ vs $7.1\pm0.9 \times 10^6$ cells/exudate; $p<0.05$) in peritoneal neutrophil recruitment and delayed the resolution of inflammation with an increased R_i to ~32h (Figure. 3a). In vagotomised mice we also found a significant reduction in *E. coli* phagocytosis by exudate leukocytes ($p<0.05$) and increased exudate bacterial counts (Figure. 3b, c).

To determine the specificity of the response elicited by the right vagus nerve in regulating peritoneal resolution tone we next investigated peritoneal host responses following resection of the left vagus nerve. Assessment of macrophage phenotypic markers demonstrated that vagotomy of the left nerve led to a significant reduction in the

expression of interleukin 10 (IL-10) and CD11b and an upregulation of cyclooxygenase (COX)-2, with the remaining macrophage markers being essentially unaltered (Figure S4a) when compared to macrophages from sham mice. Resection of the left vagus nerve did not lead to significant changes in peritoneal PCTR1 levels or macrophage and $CD335^+$ ILC3 (Figure S4b-d) numbers. When challenged with *E. coli*, mice subjected to left vagotomy gave a maximum neutrophil infiltration ($4.5 \pm 0.7 \times 10^6$ vs $5.1 \pm 0.3 \times 10^6$ neutrophils/exudate, left vagotomy vs sham) R_i (26 vs 27 h, left vagotomy vs sham) and exudate bacterial loads ($1.9 \pm 0.5 \times 10^6$ vs $3.6 \pm 1.0 \times 10^6$ CFU/exudate, left vagotomy vs sham) that were comparable to sham mice (Figure S4e,f). Together these results demonstrate that the right vagus nerve regulates peritoneal resolution tone and immunity during infections, whereas left vagal trunk disruption did not significantly alter innate immune responses to *E. coli* infections. Therefore we next sought evidence for mechanisms regulated by the right vagus nerve in regulating these host responses.

PCTR1 rescues the dysregulated inflammatory response in vagotomised mice

Having found that a reduction in peritoneal PCTR1 levels was associated with altered peritoneal macrophage phenotype and impaired host responses to infections and given the host protective actions of PCTR1 in infections (Dalli et al., 2015c; Ramon et al., 2016) we tested whether administration of PCTR1 could rectify the altered peritoneal macrophage profile. Mice were administered PCTR1 (75ng/mouse) and peritoneal lavages collected at 16h. Multivariate analysis of peritoneal $F4/80^+CD11b^+$ macrophage lineage markers demonstrated a rightward shift in the cluster representing macrophage profiles from vagotomised mice compared to sham macrophages (Figure 4a). Macrophages from vagotomised mice displayed higher expression of CD11b, F4/80 and T cell Immunoglobulin Mucin Protein (TIM-4). Administration of PCTR1 to vagotomised mice resulted in increases in several of the markers downregulated by vagus disruption

including inducible nitric oxide synthase (iNOS), Arginase (Arg)-1, and CD11c, resulting in a left ward shift in the macrophage lineage profile (Figure 4a and Table S3). This shift in peritoneal macrophage phenotype was associated with an improved ability of peritoneal macrophages to phagocytose bacteria (Figure 4b) and a reduction in several pro-inflammatory molecules including C-X-C motif ligand (CXCL)1 and the mouse homologue of interleukin 8 (KC) ($n=3$ mice per group; $p<0.05$). In addition, PCTR1 administration also led to a shift in the peritoneal lipid mediator profile (Figure 4c and Table S4). Here we found a rightward shift in the LM cluster from vagotomised mice compared to sham mice. Administration of PCTR1 to vagotomised mice reversed this shift in peritoneal lipid mediator profiles following vagotomy with the resulting lipid mediator profile cluster giving similar co-ordinates as those obtained with sham mice. This leftward shift in the LM profile clusters was accompanied by an upregulation of several SPM known to be organ protective (Serhan et al., 2015) including AT-LXA_4, RvD3 and PCTR3 and a downregulation of inflammation initiation eicosanoids (Haeggstrom and Funk, 2011; Samuelsson, 2012) such as PGD_2, $PGF_{2\alpha}$ and LTB_4 (Figure 4c and Table S4).

Since PCTR1 administration rectified peritoneal macrophage responses as well as the peritoneal lipid mediator profile in vagotomised mice, we next tested whether this was sufficient to restore the host response during infections. PCTR1 given to vagotomised mice 16h prior to *E. coli* inoculation rescued the host response, significantly reduced neutrophil recruitment as well as shortened the resolution interval from ~36h to 22 h. In comparison, the resolution interval was shortened to 16h when PCTR1 was administered to sham mice (Figure 4d). In addition, PCTR1 administration significantly upregulated *E. coli* phagocytosis by exudate leukocytes, reduced exudate bacterial loads and upregulated macrophage efferocytosis, key responses in the resolution of inflammation (Fullerton et al., 2014; Serhan et al., 2015), in both vagotomised and sham

mice (Figure 4e-f). Together these results demonstrate that PCTR1 rectifies peritoneal macrophage phenotype and host responses to *E. coli* infections in vagotomised mice.

ILC3s regulate peritoneal macrophage production of PCTR1 and accelerate resolution of infectious-inflammation

In vagotomised mice we found significant decreases in peritoneal ACh concentrations as well as in the production of PCTR1 by peritoneal macrophages (Figure 1 and 2). Given the role that these play in regulating host responses to infections we tested whether administration of cholinergic receptor agonists would rectify the macrophage phenotype and PCTR1 production. For this purpose we gave vagotomised mice carbachol, a muscarinic and nicotinic receptor agonist that is metabolically more resistant to further conversion than ACh. This upregulated the expression of macrophage lineage markers including COX-2, MHCII, CD11c and Arg-1 on peritoneal macrophages when compared to vagotomised mice (Figure 5a and Table S5). Carbachol administration did not significantly regulate peritoneal $CD335^{+}$ ILC3 numbers and PCTR1 in vagotomised mice (Figure 5b,c).

ILC3s are central in orchestrating the host immune response to bacterial infections (Mortha et al., 2014), with factors produced by these cells being important in regulating both innate and adaptive immune responses. Given that ILC3 numbers were reduced in vagotomised mice, we next questioned whether loss of these cells from the peritoneum would reduce peritoneal PCTR1 concentrations and alter macrophage phenotypes. To address this, *Rag1*$^{-/-}$ mice were either given an anti-CD90.2 antibody (*see methods*), that depleted peritoneal ILC3s by ~75% (n= 6 mice; $p<0.05$), or an isotype control. After 3 days, peritoneal lavages were obtained and assessed for peritoneal lipid mediator profiles and macrophage phenotype. Multivariate analysis of lipid mediator profiles obtained from these mice resulted in distinct lipid mediator clusters

(Figure 5d). Assessment of the loading plot demonstrated an association between CD335^{+} ILC3 and PCTR1 (Figure 5d), with concentrations of this immunoresolvent being significantly reduced in mice given the anti-CD90.2 antibody when compared to mice given an isotype antibody (Table S6a). In mice given the anti-CD90.2 antibody we also found a shift in the peritoneal macrophage phenotype as demonstrated by multivariate analysis of phenotypic markers from these mice in comparison with macrophages from mice given an isotype control antibody (Figure 5e and Table S6b).

We next tested whether these changes were associated with dysregulated host responses to infection. Mice administered the anti-CD90.2 antibody, showed significant increases in peritoneal neutrophil recruitment at each time interval, with a ~ 25% increase in Ψ_{max} and delay in the resolution interval from 18 h to 25 h compared to mice given an isotype control antibody (Figure 5f). This reduction in peritoneal ILC3 numbers was also associated with a significant decrease in exudate leukocyte phagocytosis of *E. coli*, increased peritoneal bacterial load (Figure 5g,h) and increased inflammation-initiating eicosanoids PGD_2, PGE_2, $PGF_{2\alpha}$, TXB_2 and LTB_4 (n=4 mice per group; $p<0.05$). These results demonstrated that ILC3 depletion reduced peritoneal PCTR1 and altered the phenotype of peritoneal macrophages resulting in a dysregulated host response to infections.

Acetylcholine upregulates the PCTR biosynthetic pathway in human ILC3s that promote resolution of bacterial infections

Given that lipid mediators, including PCTR1, regulate macrophage phenotype and function (Ramon et al., 2016; Serhan et al., 2015) we next tested whether ILC3s controlled peritoneal macrophage responses via SPM production. We first sorted mouse ILC3 (~98% purity, Figure S1b) and assessed the expression of 12/15-lipoxygenase

(LOX), a key enzyme in pro-resolving mediator biosynthesis. Realtime qPCR (n = 3 mice) and flow cytometric analysis of mouse CD335^{+} ILC3s demonstrated that these cells expressed the murine homologue of this enzyme (Figure 6a). In addition, realtime quantitative PCR analysis of these sorted cells demonstrated that they also expressed the cholinergic receptors Cholinergic Receptor, Muscarinic (*Chrm*) 1, *Chrm2*, *Chrm4* and *Chrm5* (n=3 mice). Incubation of CD335^{+} ILC3 with ACh, a key vagus derived neurotransmitter (Vartiainen, 1934), upregulate the levels of the PCTR1 pathway marker 17-hydroxy-4Z,7Z,10Z,13Z,15E,19Z-docosahexaenoic acid (17-HDHA; Figure 6b).

We next tested whether these cells were responsible for regulating peritoneal macrophage PCTR1 production in vagotomised mice. Incubation of peritoneal macrophages with peritoneal CD335+ILC3s (sorted as illustrated in Figure S2b) resulted in increased PCTR1 production when compared to mice incubated with vehicle alone, and this action was reversed when ILC3 were incubated with a lipoxygenase inhibitor prior to incubation with peritoneal macrophages (Figure 6c). Given these actions we investigate potential sites within the peritoneum where the crosstalk between cholinergic nerves, ILC3s and macrophages could occur. Given the role of the greater omentum in leukocyte trafficking to the peritoneum (Fukatsu et al., 1996) and that the right vagus nerve fibers terminate in gastroepiploic plexus, the location of neural cell bodies that project axons in the gastroepiploic nerve that innervate this organ, (Swanson, 2015) we assessed whether these interactions may occur in the greater omentum. Using confocal microscopy we identified RoRγt^{+}CD3^{-} cells in close proximity to choline acetyltransferase positive cells and F4/80^{+} cells (Figure 6d).

Since PCTR1 displays potent host protective actions we next tested whether adoptive transfer of ILC3 would rectify the dysregulated host response in vagotomised mice. To this end, we sorted mouse ILC3s from enrich splenocytes populations following the gating strategy illustrated in Figure S5. These cells were then adoptively transferred

via i.p. injection to vagotomised animals 3h prior to *E. coli* inoculation and resolution indices were calculated. ILC3 administration led to a significant decreases in neutrophil recruitment, shortened the resolution interval from ~38 h to ~23 h and reduced peritoneal bacterial loads when compared to vagotomised mice given only vehicle (Figure 6e, f). These protective actions were lost when ILC3s were incubated with a lipoxygenase inhibitor prior to administration to mice, thus supporting a role for ILC3-derived SPMs in regulating peritoneal resolution tone and host responses to infections.

To test whether these findings had translational relevance in humans, we next assessed whether human $FSC^{low}SSC^{low}LIN^{-}CD127^{+}$ $CD161^{+}$ $ROR\gamma t^{+}CD56^{+}CD336^{+/-}$ ILC3s expressed 15-LOX type 1, the human homologue to mouse 12/15-LOX in the PCTR biosynthetic pathway. Using flow cytometry (Figure 6g, Figure S6) and real-time qPCR (n=4 donors) we found that human ILC3s expressed this SPM biosynthetic enzyme. Incubation of human ILC3s with ACh also significantly upregulated 17-HDHA levels (41.7±7.4 vs 113±13.1 pg/1x10^6 cells; ILC3 vs ILC3+Ach; $p<0.01$). To further underpin the role of SPMs in mediating the protective actions of ILC3s and rule out the contribution of proteins in mediating these actions, we administered human ILC3s to mice 3h prior to infections. Human ILC3s were incubated with ACh and then administered to vagotomised mice, and this led to a significant reduction in neutrophil numbers in peritoneal exudates and shortening of the resolution interval from by ~10 h, compared to vagotomised mice given only vehicle (Figure 6h). These protective actions were lost when ILC3s were incubated with a lipoxygenase inhibitor prior to administration to vagotomised mice. Together these results demonstrate that ILC3s regulate peritoneal resolution tone and host responses to bacterial infections via SPMs, upregulating peritoneal macrophage PCTR1 levels and promoting the resolution of infectious-inflammation.

Discussion

Results from the present report detail a resolution circuit regulated by the vagal system that involves pro-resolving mediators, ILC3s and resident peritoneal macrophages. Disruption of the vagal system lead to an alteration in the cellular composition of resident innate immune cells in the peritoneum as well as a shift in the phenotype of tissue resident macrophages. In addition, vagotomy resulted in an altered peritoneal lipid mediator profile with decreased in the tissue protective and immunoresolvent PCTR1, and increased concentrations of inflammation initiating eicosanoids. Vagotomy also delayed the resolution of *E. coli*-initiated bacterial infection. This delay in infection-resolution was rescued by administration of either mouse or human ILC3s or PCTR1, which limited neutrophil infiltration to the site of infection, restored peritoneal macrophage responses and enhanced the containment and clearance of bacteria. Together these findings indicate that ILC3s and PCTR1 are actively involved in regulating the tissue resolution capacity establishing a resolution circuit that is under the control of the central nervous system.

Regulation of peripheral host responses to injury or infection is now appreciated to be under the control of the nervous system, with the efferent vagal nerve involved in coordinating cellular recruitment and actions at the inflamed site (Pavlov and Tracey, 2015). Disruption of the vagal system leads to a dysregulated host response and disease propagation following both sterile and infectious insults (Mirakaj et al., 2014; Pavlov and Tracey, 2015; Rosas-Ballina et al., 2011). This regulation is in part mediated via the release of ACh by the vagus that regulates innate and adaptive immune cell responses during inflammation (Pavlov and Tracey, 2015). Recently we reported that the vagus also regulates resolution responses during sterile inflammation by modulating local levels of the neuronal guidance molecule netrin-1 as well as RvD1, RvD3 and PD1 (Mirakaj et al., 2014). In the present study we found that the vagus also played a critical

role in regulating the resolution tone of the peritoneum, whereby vagotomy led to a significant increase in resident peritoneal macrophage numbers, a shift in their phenotype to a pro-inflammatory phenotype and a reduced ability to phagocytose bacteria. In these mice we also found a significant reduction in peritoneal ILC3 numbers and a shift in the peritoneal lipid mediator profile prior to challenge, with an increase in inflammation initiation eicosanoids and a reduction in PCTR1. In addition, vagotomy led to a disruption of resolution responses to pathogenic *E. coli* characterized by increased leukocyte recruitment, exudate inflammatory eicosanoids at the peak of inflammation (n = 5-6 mice per group; $p<0.05$), a reduction in the ability of exudate leukocytes to phagocytose bacteria and a delay in the resolution of infectious inflammation.

Tissue resident cells provide the first line of defense against infections with innate cells paying a critical role in initiating the inflammatory response (Kim and Luster, 2015). In the peritoneum, resident macrophages are key players in orchestrating the initiation of the inflammatory response. Upon recognition of an inflammatory stimulus (e.g. bacteria) these cells produce a host of inflammatory signals including cytokines and lipid mediators that lead to vascular leakage and leukocyte recruitment (Hellmann et al., 2015). In addition, these cells also actively participate in clearance of invading pathogens and alteration in their phenotype impairs their ability to clear bacteria and leads to a dysregulated inflammatory response in experimental systems (Dahdah et al., 2014) and humans (Ahmed et al., 2014). In the present study we found that administration of PCTR1 to vagotomised mice 16h prior to challenge at a dose as low as 75ng/mouse restored the macrophage phenotype as well as phagocytic function. In addition, this immunoresolvent also rectified the dysregulated peritoneal resolution responses in vagotomised mice indicating a central role for PCTR1 in regulating the resolution tone in this tissue and in promoting the resolution of infectious-inflammation.

It is now appreciated that tissue resident ILC3s actively regulate macrophage responses in infections *via* the production of cytokines such as. GM-CSF (Mortha et al., 2014). In the present experiments, we found that murine and human ILC3 expressed the initiating enzyme in the production of PCTR1 and that incubation of ILC3s with ACh led to an increase in 17-HDHA, the biosynthetic pathway marker in the PCTR metabolome. In this context the actions of ACh on ILC3 may have been mediated by at least one of the cholinergic receptors Chrm1, Chrm2, Chrm4 and Chrm5 expressed by these cells. Depletion of ILC3s in *Rag1*$^{-/-}$ mice led to a dysregulated peritoneal lipid mediator profile, a reduction in PCTR1 concentrations, an alteration of the peritoneal macrophage phenotype and a delay in the resolution of infectious inflammation. Administration of human or mouse ILC3s prior to bacterial infection restored resolution responses in vagotomised mice, an action that was inhibited when these cells were pre-incubated with a lipoxygenase inhibitor. These results demonstrated that ILC3s carry the biosynthetic machinery necessary for the production of pro-resolving mediators. They also demonstrated that ACh, a central mediator in the vagal response, regulates the PCTR biosynthetic pathway in ILC3s that may in turn regulate resident peritoneal macrophage responses.

Therefore several lines of evidence were employed to determine the role of the right vagus in controlling peritoneal resolution tone and host responses to infections via ILC3 and PCTR1. They are as follows: **i)** vagotomy reduced peritoneal PCTR1 levels prior to bacterial challenge; **ii**) Resection of the right vagus trunk reduces peritoneal ILC3 counts and alters peritoneal macrophage phenotype; **iii)** vagotomized mice had an exacerbated inflammatory response, delayed resolution and in efficient bacterial clearance in response to *E. coli* infections; **iv)** peritoneal macrophage derived PCTR1 accounted for ~ 70% of peritoneal PCTR1 levels in sham mice; **v)** PCTR1 administration to vagotomised mice restored peritoneal macrophage phenotype and responses to

infection and partially rescued the peritoneal lipid mediator profile; **vi)** Administration of carbachol, a nicotinic and muscarinic agonist, to vagotomized mice did not restore peritoneal ILC3 numbers and PCTR1 levels and only partly restored peritoneal macrophage phenotype;.**vii)** ILC3 depletion in $Rag1^{-/-}$ mice gave reduced peritoneal PCTR1, alteration of the resident peritoneal macrophage phenotype and delayed resolution responses to infection; **viii)** ILC3 express the initiating enzyme in the PCTR1 biosynthetic pathway and incubation of ILC3 with acetylcholine upregulated the PCTR1 pathway; **ix)** ILC3, macrophages and cholinergic cells are found in close proximity in the greater omentum; **x)** Incubation of peritoneal macrophage from vagotomised mice with ILC3 upregulated macrophage PCTR1 production, an action that was reversed when ILC3 we incubated with a lipoxygenase inhibitor **xi)** Addback of human and mouse ILC3 restored host responses to *E. coli* infections in vagotomized mice, protective actions that were lost when ILC3 were incubated with a lipoxygenase inhibitor.

In summation, the present results identify neural-regulated ILC3 pro-resolving mediator production that contributes to maintaining local homeostatic tissue tone and expedites resolution of bacterial infections. These results elucidate a mechanism for peripheral neuronal control in regulating ILC3 responses and PCTR1 production that orchestrate host responses during infections. Thus these results indicate that impairment of the cholinergic system, as for example found in aging, diminishes pro-resolving mediator production by resident leukocytes leading to an altered tissue resolution tone and blunted resolution responses to infectious challenge. These findings may be useful in designing therapeutics for treating infectious-inflammation that spares the immune response.

Experimental Procedures

E. coli peritonitis

All animal experiments were conducted in accordance with the Harvard Medical Area Standing Committee on Animals (protocol no. 02570) and UK Home Office regulations (Guidance on the Operation of Animals, Scientific Procedures Act, 1986). Mice (male FvB, 6-8 weeks old, Charles River, fed lab diet containing essential fatty acids as from supplier) were anesthetized and cervical vagotomy or sham surgery were performed 7 days before induction of peritonitis (Mirakaj et al., 2014). In brief, mice were anesthetized and a ventral cervical midline incision was performed to expose the right cervical vagus trunk, which was ligated with a 4.0 silk suture and then divided. 1, 3 or 7 days later, peritoneal lavages and organ tissues were obtained. In select experiments 7 day after vagotomy peritonitis was initiated by intraperitoneal injection of *E. coli* (serotype O6:K2:H1; $1x10^6$ CFU/mouse). At designated time intervals mice were harvested, blood was collected via cardiac puncture in heparin, and peritoneal exudates were collected by injecting in 4ml of PBS intraperitoneally and ~ 3ml of PBS were recovered. The **cellular composition** in the exudates was determined using Turks solution and light microscopy, and flow cytometry. For **flow cytometry,** exudate cells were incubated with anti-mouse CD16/CD32 (eBiosciences, 20min, 4^oC, in PBS containing 5% fetal calf serum-staining solution), followed by incubation with lineage specific markers for 30min (4^oC, in staining solution). Cell counts for each population were then calculated by multiplying the total cell counts obtained using light microscopy and the percentage of each population as determined by flow cytometry and the normalized to 4ml of PBS that was initially injected.

Flow cytometry

Mouse cells were incubated with anti-mouse CD16/CD32 (eBiosciences, 20min, 4°C, in PBS containing 5% fetal calf serum-staining solution), followed by incubation with lineage specific markers for 30min (4^{o}C, in staining solution), all antibodies were purchased from BioLegend unless otherwise stated. Multiparameter analysis was performed on FACS Canto II (BD), BD LSR Fortessa and BD FACSAria II and analysis was conducted using FlowJo (Tree Star). For staining of intracellular components we incubated cell with Foxp3-staining kit (eBioscience) according to the manufacturer's instructions prior to addition of fluorescently labeled antibodies. Dead cells were excluded using LIVE/DEAD Fixable Yellow Dead Cell Stain (Invitrogen, Carlsbad, CA). For neutrophil analysis the following antibodies were employed: PE-anti-Ly6G (clone: 1A8), PE/Cy5.5-anti-CD11b (clone: M1/70). For macrophage phenotypic analysis we used the following antibodies: PE-Cy7-anti-CD11b (clone: M1/70), Brilliant Violet (BV) 650-anti MHCII (clone: M5/114.15.2) APC-Cy7-anti-F4/80 (clone: BM8), PE-Dazzle 594-anti-IL10 (clone: JES5-16E3), BV-421-anti-TGFβ (clone: TW7-16B4), BV785-anti-CD11c (clone: N418), Alexa-647-anti-Tim4 (clone: F31-5G3), FITC-anti-COX-2 (Cayman Chemicals; Cat no: 10010096), PE-anti-Arg-1 (R&D Systems, Cat no: IC5868P), Alexa Fluor 488-anti-iNOS (clone: CXNFT).

For *T-cell* analysis the following antibody was used: FITC-anti-CD3 (clone: 17A2). For *B-cell* analysis the following antibodies were used PE-anti-CD19 (clone: 6D5) and APC-anti-B220 (clone: RA3-6B2). *ILC3* populations were determined using the following antibodies: FITC-anti-CD3 (clone: 17A2), FITC-anti-CD19 (clone: 6D5), FITC-anti-CD11c (clone: N418), FITC-anti-Ly6G (clone: 1A8), FITC-anti-F4/80 (clone: BM8), FITC-anti-CD14 (clone: Sa14-2), Alexa Fluor 647-anti-RORγt (clone: Q31-378; BD Pharmingen), BV711-anti-NK1.1 (clone: PK136), BV650-anti-CD127 (clone: A7R34),

PE-anti-IL23R (clone: 753317; R&D Systems), PE-Cy7-anti-CD117 (clone: 2B8; BioLegend) and BV421-anti-CD335 (clone: 29A1.4).

ILC3 fluorescence-activated cell sorting

For sorting of human ILC3 blood peripheral blood mononuclear cells (PBMC) were purchased from Children's Hospital Blood Bank, Boston and cells enriched using an EasySep^{TM} Human NK cell enrichment kit (Stemcell Technologies) following manufacturers instructions. Subsequently cells were incubated with LIVE/DEAD Fixable Yellow Dead Cell Stain (Invitrogen) following manufactures instruction then with the following antibody combination: FITC-anti-CD3 (clone: UCHT1), FITC-anti-CD19 (clone: HIB19, FITC-anti-CD14 (clone: HCD14), FITC-anti-CD20 (clone: 2H7), FITC-anti-CD1a (clone: HI149), FITC-anti-CD34 (clone: 581), FITC-anti-TCR α/β (clone: IP26), FITC-anti-CD94 (clone: DX22), PE-Cy7-anti-CD161 (clone: HP-3G10), BV711-anti-CD117 (clone: 104D2), PE-CF594-anti-CD294 (clone: BM16; BD Bioscience) and eFluor450-anti-CD336 (clone: 44.189; eBioscience). In select experiments sorted cells were incubated with Foxp3-staining kit (eBioscience) according to the manufacturer's instructions and then Alexa Fluor-647-anti-RORγt (clone: Q21-559; BD Bioscience), or with an Alexa Fluor-647-anti-15-LOX-1 (Bioss: cat no: bs-6505R-A647).

For sorting of mouse cells, spleens were gently dispersed using a 70μm strainer, cells were then enriched using an EasySep^{TM} MouseNK cell enrichment kit (Stemcell Technologies) following manufacturers instructions. Subsequently cells were incubated with LIVE/DEAD Fixable Yellow Dead Cell Stain (Invitrogen) following manufactures instruction then with the following antibody combination: FITC-anti-CD3 (clone: 17A2), FITC-anti-CD19 (clone: 6D5), FITC-anti-CD11c (clone: N418), FITC-anti-Ly6G (clone: 1A8), FITC-anti-F4/80 (clone: BM8), FITC-anti-CD14 (clone: Sa14-2), BV711-anti-NK1.1 (clone: PK136), BV510-anti-CD127 (clone: A7R34), PE-anti-IL23R (clone: 753317; R&D

Systems) and BV421-anti-CD335 (clone: 29A1.4). In select experiments sorted cells were incubated with Foxp3-staining kit (eBioscience) according to the manufacturer's instructions and then with an anti-15-LOX-1 (Bioss: cat no: bs-6505R) then with an Alexa Fluor-647-anti-15-LOX-1 (Bioss: cat no: bs-6505R-A647).

Lipid mediator profiling

Peritoneal lavages and infectious exudates were placed in 2 volumes of ice-cold methanol. Samples for LC-MS-MS-based metabololipidomics were extracted with solid-phase extraction columns (Colas et al., 2014). Briefly, prior to sample extraction, deuterated internal standards (d_4-PGE_2, d_5-LXA_4, d_4-RvD2, d_4-LTB_4, d_5-LTC_4, d_5-LTD_4, d_5-LTE_4 and d_8-5S-HETE) representing regions of interest in chromatographic analysis (500 pg each) were added to facilitate quantification. Eluted methyl formate fractions were analyzed by a LC-MS-MS system, Qtrap 5500 (AB Sciex) equipped with a Shimadzu SIL-20AC autoinjector and LC-20AD binary pump (Shimadzu Corp.). An Agilent Eclipse Plus C18 column (100x4.6mmx1.8µm) was used with a gradient of methanol/water/acetic acid of 55:45:0.01 (vol:vol:vol) that was ramped to 85:15:0.01 (vol:vol:vol) over 10 min and then to 98:2:0.01 (vol:vol:vol) for the next 8 min. This was subsequently maintained at 98:2:0.01 (vol:vol:vol) for 2 min. The flow rate was maintained at 0.4ml/min. To monitor and quantify the levels of lipid mediators, a multiple reaction monitoring (MRM) method was developed with signature ion fragments (m/z) for each molecule monitoring the parent ion (Q1) and a characteristic daughter ion (Q3). Identification was conducted using published criteria where a minimum of 6 diagnostic ions were employed (Colas et al., 2014). Calibration curves were determined using a mixture of lipid mediators obtained via total organic synthesis. Linear calibration curve for each compound was obtained with r^2 values ranging from 0.98 to 0.99. Detection limit was ~0.1 pg. Quantification was carried out as in (Colas et al., 2014).

For identification and quantification of PCTRs and cysteinyl leukotrienes, methanol fractions were taken to the LC-MS-MS system operated as described (Dalli et al., 2015c) with minor modifications. A Shimadzu LC-20AD HPLC and a Shimadzu SIL-20AC autoinjector paired with a QTrap 5500 (AB SCIEX) were used. A Poroshell 120 EC-C18 column (100 mm × 4.6 mm × 2.7 μm; Agilent) was kept in a column oven at 50 °C (Therma Sphere; TS-130), and lipid mediators were eluted with a mobile phase consisting of methanol/water/acetic acid at 55:45:0.1 (vol:vol:vol) that was isocratic for 1 min, ramped to 70:30:0.1 (vol:vol:vol) over 5 min, then to 80:20:0.1 (vol:vol:vol) for 2 min, then isocratic 80:20:0.1 (vol:vol:vol) for the next 3 min, and ramped to 98:2:0.1 (vol:vol:vol) over 3 min. This was subsequently maintained at 98:2:0.1 (vol:vol:vol) for 3 min, and the flow rate was maintained at 0.6 ml/min. The QTrap 5500 was operated in positive ionization mode using scheduled multiple reaction monitoring (MRM) coupled with information-dependent acquisition and enhanced product ion scan. For complete chemical nomenclature for the SPM and other lipid mediators identified herein, see (Colas et al., 2014; Dalli et al., 2015c).

Macrophage incubations

Peritoneal macrophages from sham, vagotomised mice and vagotomised mice given PCTR1 were collected in 4 ml of DPBS (without calcium and magnesium), cells were counted and seeded ($5x10^4$ cells/well) in 96 well plates and allowed to adhere for 2h at 37^oC. Non-adherent cells were washed and cells incubated with fluorescently labeled bacteria and phagocytosis was assessed using a Zeiss YFL (Carl Zeiss, Thornwood, NY, USA) and ImagePro Plus 7 software (Media Cybernetics, Bethesda, MD, USA) and SpectraMax M3 plate reader (Molecular Devices Inc, Sunnyvale, CA) and results analyzed using SoftMax Pro (Molecular Devices Inc, Sunnyvale, CA)(Chiang et al., 2012).

In select experiments macrophages ($2x10^5$ cells/well) were plated in 12 well plates, incubated for 2h at 37°C to allow for adhesion, non-adherent cells were washed off and cells incubated with *E. coli* ($1x10^7$ CFU/well) for 6h at 37°C. Supernatants were then collected and centrifuged at 10,000x*g* for 10 min to remove any cellular debris and cytokine levels were assessed using a Proteome Profiler™ Mouse XL Cytokine Array Kit (R&D systems) following manufacturers instructions.

In separate experiments macrophages from sham or vagotomised mice 1, and 7 days post vagotomy were plated in 6 well plates ($1x10^6$ cells/well, 45 min, 37°C, $PBS^{+/+}$). Cells incubations were quenched using ice-cold methanol containing deuterium labeled internal standards and lipid mediators identified and quantified as detailed above.

To investigate whether CD335+ ILC3 regulate macrophage responses, macrophages were isolated from vagotomised mice 2 days post vagotomy, cells were plated in 6 well plates ($1x10^6$ cells/well, 45 min, 37°C, $PBS^{+/+}$). Non-adherent cells were removed and cells incubated with $CD335^+$ ILC3 ($7.5x10^2$ cells/well, 6h, 37°C, $PBS^{+/+}$, 2% FCS). Incubations were quenched using ice-cold methanol containing deuterium labeled internal standards and PCTR1 was identified and quantified as detailed above.

Statistics

All results are expressed as means ± SEM. We assumed normality and equal distribution of variance between the different groups analyzed. The experiments were conducts and analysed using a factorial design. Differences between groups were compared using Student's t test (2 groups), 1-way ANOVA and 2-way ANOVA (multiple groups) followed by post hoc Bonferroni test. Investigators were not blinded to group allocation or outcome assessment. Sample sizes for each experiment were determined on the variability observed in preliminary experiments and prior experience with the experimental systems. The criterion for statistical significance was $p<0.05$. PLS-DA

analysis was conducted using SIMCA 13.0.3 software (Umetrics, San Jose, CA) as described in (Colas et al., 2014) with mediators and macrophage lineage markers giving Variable Importance in Projection scores greater than 1 taken as displaying significant correlation. This parameter estimates the importance of a variable in the Partial Least Square projections with scores greater then 1 indicating that a specific variable is important in a given model.

Author Contributions

J.D., R.C and H.A. designed and carried out experiments and analyzed data; J.D. and C.N.S. conceived the overall research plan and experimental design. All authors contributed to manuscript and figure preparation.

Acknowledgments

This work was supported by the National Institutes of Health (P01GM095467 and GM38765 to C.N.S.). J. D. received funding from the European Research Council (ERC) under the European Union's Horizon 2020 research and innovation programme (grant agreement No 677542). J.D. is also supported by a Sir Henry Dale Fellowship jointly funded by the Wellcome Trust and the Royal Society (grant 107613/Z/15/Z).
The authors declare no competing financial interests.

References:

Ahmed, A.M., Kadaru, A.G., Omer, I., Musa, A.M., Enan, K., El Khidir, I.M., and Williams, R. (2014). Macrophages from patients with cirrhotic ascites showed function alteration of host defense receptor. Journal of clinical and experimental hepatology *4*, 279-286.

Campbell, E.L., MacManus, C.F., Kominsky, D.J., Keely, S., Glover, L.E., Bowers, B.E., Scully, M., Bruyninckx, W.J., and Colgan, S.P. (2010). Resolvin E1-induced intestinal alkaline phosphatase promotes resolution of inflammation through LPS detoxification. Proceedings of the National Academy of Sciences of the United States of America *107*, 14298-14303.

Chiang, N., Fredman, G., Backhed, F., Oh, S.F., Vickery, T., Schmidt, B.A., and Serhan, C.N. (2012). Infection regulates pro-resolving mediators that lower antibiotic requirements. Nature *484*, 524-528.

Colas, R.A., Shinohara, M., Dalli, J., Chiang, N., and Serhan, C.N. (2014). Identification and signature profiles for pro-resolving and inflammatory lipid mediators in human tissue. Am J Physiol Cell Physiol *307*, C39-54.

Dahdah, A., Gautier, G., Attout, T., Fiore, F., Lebourdais, E., Msallam, R., Daeron, M., Monteiro, R.C., Benhamou, M., Charles, N.*, et al.* (2014). Mast cells aggravate sepsis by inhibiting peritoneal macrophage phagocytosis. The Journal of clinical investigation *124*, 4577-4589.

Dalli, J., Chiang, N., and Serhan, C.N. (2015a). Elucidation of novel 13-series resolvins that increase with atorvastatin and clear infections. Nat. Med. *21*, 1071-1075.

Dalli, J., Kraft, B.D., Colas, R.A., Shinohara, M., Fredenburgh, L.E., Hess, D.R., Chiang, N., Welty-Wolf, K., Choi, A.M., Piantadosi, C.A., and Serhan, C.N. (2015b). The Regulation of Proresolving Lipid Mediator Profiles in Baboon Pneumonia by Inhaled

Carbon Monoxide. American journal of respiratory cell and molecular biology *53*, 314-325.

Dalli, J., Ramon, S., Norris, P.C., Colas, R.A., and Serhan, C.N. (2015c). Novel proresolving and tissue regenerative resolvin and protectin sulfido-conjugated pathways. FASEB J. *29*, 2120-2136.

Dinarello, C.A. (2011). Interleukin-1 in the pathogenesis and treatment of inflammatory diseases. Blood *117*, 3720-3732.

Flannigan, K.L., Agbor, T.A., Blackler, R.W., Kim, J.J., Khan, W.I., Verdu, E.F., Ferraz, J.G., and Wallace, J.L. (2014). Impaired hydrogen sulfide synthesis and IL-10 signaling underlie hyperhomocysteinemia-associated exacerbation of colitis. Proceedings of the National Academy of Sciences of the United States of America *111*, 13559-13564.

Fukatsu, K., Saito, H., Han, I., Yasuhara, H., Lin, M.T., Inoue, T., Furukawa, S., Inaba, T., Hashiguchi, Y., Matsuda, T., and Muto, T. (1996). The greater omentum is the primary site of neutrophil exudation in peritonitis. J Am Coll Surg *183*, 450-456.

Fullerton, J.N., O'Brien, A.J., and Gilroy, D.W. (2014). Lipid mediators in immune dysfunction after severe inflammation. Trends Immunol *35*, 12-21.

Gao, Y., Min, K., Zhang, Y., Su, J., Greenwood, M., and Gronert, K. (2015). Female-Specific Downregulation of Tissue Polymorphonuclear Neutrophils Drives Impaired Regulatory T Cell and Amplified Effector T Cell Responses in Autoimmune Dry Eye Disease. Journal of immunology *195*, 3086-3099.

Haeggstrom, J.Z., and Funk, C.D. (2011). Lipoxygenase and leukotriene pathways: biochemistry, biology, and roles in disease. Chemical reviews *111*, 5866-5898.

Hellmann, J., Tang, Y., Zhang, M.J., Hai, T., Bhatnagar, A., Srivastava, S., and Spite, M. (2015). Atf3 negatively regulates Ptgs2/Cox2 expression during acute inflammation. Prostaglandins & other lipid mediators *116-117*, 49-56.

Kim, N.D., and Luster, A.D. (2015). The role of tissue resident cells in neutrophil recruitment. Trends in immunology *36*, 547-555.

Lee, C.R., and Zeldin, D.C. (2015). Resolvin Infectious Inflammation by Targeting the Host Response. The New England journal of medicine *373*, 2183-2185.

Leoni, G., Neumann, P.A., Kamaly, N., Quiros, M., Nishio, H., Jones, H.R., Sumagin, R., Hilgarth, R.S., Alam, A., Fredman, G.*, et al.* (2015). Annexin A1-containing extracellular vesicles and polymeric nanoparticles promote epithelial wound repair. The Journal of clinical investigation *125*, 1215-1227.

Leslie, M. (2015). Inflammation's stop signals. Science *347*, 18-21.

Mirakaj, V., Dalli, J., Granja, T., Rosenberger, P., and Serhan, C.N. (2014). Vagus nerve controls resolution and pro-resolving mediators of inflammation. The Journal of experimental medicine *211*, 1037-1048.

Mortha, A., Chudnovskiy, A., Hashimoto, D., Bogunovic, M., Spencer, S.P., Belkaid, Y., and Merad, M. (2014). Microbiota-dependent crosstalk between macrophages and ILC3 promotes intestinal homeostasis. Science *343*, 1249288.

Nakamura, M., and Shimizu, T. (2011). Leukotriene receptors. Chemical reviews *111*, 6231-6298.

Nathan, C. (2012). Fresh approaches to anti-infective therapies. Sci. Transl. Med. *4*, 140sr142.

Pavlov, V.A., and Tracey, K.J. (2012). The vagus nerve and the inflammatory reflex--linking immunity and metabolism. Nature reviews. Endocrinology *8*, 743-754.

Pavlov, V.A., and Tracey, K.J. (2015). Neural circuitry and immunity. Immunologic research *63*, 38-57.

Proia, R.L., and Hla, T. (2015). Emerging biology of sphingosine-1-phosphate: its role in pathogenesis and therapy. The Journal of clinical investigation *125*, 1379-1387.

Ramon, S., Dalli, J., Sanger, J.M., Winkler, J.W., Aursnes, M., Tungen, J.E., Hansen, T.V., and Serhan, C.N. (2016). The Protectin PCTR1 Is Produced by Human M2 Macrophages and Enhances Resolution of Infectious Inflammation. The American journal of pathology *186*, 962-973.

Rosas-Ballina, M., Olofsson, P.S., Ochani, M., Valdes-Ferrer, S.I., Levine, Y.A., Reardon, C., Tusche, M.W., Pavlov, V.A., Andersson, U., Chavan, S.*, et al.* (2011). Acetylcholine-synthesizing T cells relay neural signals in a vagus nerve circuit. Science *334*, 98-101.

Samuelsson, B. (2012). Role of basic science in the development of new medicines: examples from the eicosanoid field. J. Biol. Chem. *287*, 10070-10080.

Serhan, C.N., Chiang, N., and Dalli, J. (2015). The resolution code of acute inflammation: Novel pro-resolving lipid mediators in resolution. Seminars in immunology *27*, 200-215.

Swanson, L.W. (2015). Neuroanatomical terminology : a lexicon of classical origins and historical foundations.

Tabas, I., and Glass, C.K. (2013). Anti-inflammatory therapy in chronic disease: challenges and opportunities. Science *339*, 166-172.

Vartiainen, A. (1934). Does vagus stimulation cause an increase in the acetylcholine content of heart muscle? J Physiol *82*, 282-292.

Ward, P.A. (2012). New approaches to the study of sepsis. EMBO molecular medicine *4*, 1234-1243.

Figure Legends

Figure 1: Vagotomy diminishes PCTR1 concentrations and elevated eicosanoids in peritoneum.

Mice were subjected to right unilateral vagotomy or sham surgery, at the indicated intervals the peritoneal cavity was lavaged and lipid mediators profiled using LC-MS-MS based LM metabololipidomics (see methods for details). (a) Representative multiple reaction chromatograms for identified lipid mediators, and (b) MS-MS spectrum employed in the identification of PCTR1. (c) Lipid mediator profiles were then interrogated using Partial least square discriminant analysis (PLS-DA). *Top panel:* 2D score plot *bottom panel:* 2D loading plot. (d) Peritoneal acetylcholine levels. Results for a-c are representative of n=5-6 mice per group from two distinct experiments. Results for d are mean ± s.e.m. n=4-5 mice per group **p<0.01 vs Sham mice. m/z = mass to charge ratio.

Figure 2: Resident peritoneal ILC3 numbers are reduced and peritoneal macrophage phenotype is altered in vagotomised mice. Mice were subjected to unilateral vagotomy or sham surgery, and peritoneal cells were collected at the indicated intervals. (a) ILC3 and (b) macrophage numbers were determined using light microscopy and flow cytometry. (c) Peritoneal macrophage phenotypic marker expression was determined using flow cytometry and results interrogated using PLS-DA. *Top panel:* 2D score plot *bottom panel:* 2D loading plot. (d) Peritoneal macrophages were isolated and lipid mediators determined using lipid mediator profiling. Results were then interrogated using PLS-DA. *Top panel:* 2D score plot *bottom panel:* 2D loading plot. Results for a, b are mean ± s.e.m. 4-5 mice per group from two distinct experiments. Results for c, d are representative of 3-4 mice per group. Related to Figure S2, S3 and Table S1, S2

Figure 3: Vagotomy delayed resolution of infections. Mice were subjected to unilateral vagotomy or sham surgery; after 7 days *E. coli* ($1x10^6$ CFU/mouse) were administered via i.p. injection. Inflammatory exudates were collected at the indicated intervals: (a) cell counts determined using light microscopy and flow cytometry and resolution indices calculated. (b) Exudate leukocyte phagocytosis of *E. coli* ($CD11b^+$ *E. coli*$^+$ cells) was determined by flow cytometry in 12h exudates (c) 12h exudate bacterial loads. Results are mean ± s.e.m. n= 4 mice per group from two distinct experiments. Related to Figure S3

Figure 4: PCTR1 restores resolution responses in vagotomised mice during bacterial infections. (a-c) Mice were subjected to unilateral vagotomy or sham surgery, after 7 days vagotomised mice were administered vehicle (saline containing 0.01% EtOH) or PCTR1 (75ng/mouse) via i.p. injection. After 16h (a) peritoneal lavages were collected and macrophage phenotype was determined using flow cytometry and (b) peritoneal LM profiles were determined using LM metabololipidomics. (c) peritoneal cells were collected, plated in 96-well plates ($5x10^4$ cells/well; DPBS; 2h; 37^{o}C) then incubated with fluorescently labeled *E. coli* ($2.5x10^6$ CFU/well; 37^{o}C, $PBS^{+/+}$, pH 7.45, 40 min) and phagocytosis assessed using a fluorescence microscopy. Results are representative of n= 5-6 mice per group from two distinct experiments. (d-g) Mice were administered *E. coli* ($1x10^6$ CFU/mouse, i.p.), (d) exudates collected at the indicated intervals and neutrophil count determined using flow cytometry and light microscopy. (e) 12h Exudate leukocyte *E. coli* phagocytosis determined as $CD11b^+$ *E. coli*$^+$ cells, (f) 12h exudate bacterial loads and (g) 24h exudate macrophage efferocytosis determined as $F4/80^+$ $Ly6G^+$ cells. Results for c are mean±s.e.m. n= 5-6 mice per group from two distinct experiments. Related to Table S3 and S4

Figure 5: ILC3 regulate peritoneal macrophage phenotype, PCTR1 production and resolution of infectious-inflammation. Mice were subjected to right unilateral vagotomy or sham. Vagotomised mice were then administered vehicle (Vagotomy; PBS) or Carbachol (Vagotomy+Carbachol; 0.1mg/Kg/day for 7days). Peritoneal lavages were collected (a) expression of macrophage phenotypic markers (b) $CD335^{+}$ ILC3 and (c) PCTR1 levels determined. Results for a are representative of n=3 mice per group. Results for b,c are mean±sem of n=3 mice per group. * $p<0.05$. (d-e) $Rag1^{-/-}$ mice were administered an anti-CD90.2 (250µg/mouse) or Isotype control (250µg/mouse) antibody, (d) peritoneal lavages were collected and lipid mediator profiles determined using LC-MS-MS based LM metabololipidomics and PLS-DA. *Left panel* 2D score plot, *right panel* 2D loading plot. (e) Peritoneal macrophages were collected and phenotypic marker expression determined using flow cytometry. *Left panel* 2D score plot, *right panel* 2D loading plot. Results are representative of n= 4 mice per group from two distinct experiments. (f-h) $Rag1^{-/-}$ mice were administered an anti-CD90.2 (250µg/mouse) or Isotype control (250µg/mouse) antibody. After 3 days they were given *E. coli* ($1x10^{5}$ CFU/mouse) via i.p. injection, exudates collected at the indicated intervals and (f) cell counts were determined using light microscopy and flow cytometry and resolution indices calculated. (g) Exudate leukocyte phagocytosis of *E. coli* ($CD11b^{+}$ *E. coli*$^{+}$ cells) was determined by flow cytometry in 12h exudates. (h) 12h exudate bacterial loads. Results are mean ± s.e.m. n= 4 mice per group from two distinct experiments. Related to Table S6

Figure 6: Acetylcholine upregulates SPM biosynthetic pathways in human and mouse ILC3 that restore peritoneal host responses to infections in vagotomised mice. (a) Expression of mouse 12/15-LOX in mouse $CD335^{+}$ ILC3 (b) mouse ILC3 were

isolated using FACS sorting (see methods) then incubated with DHA (300ng/ml) then with ACh (1nM, 37^{o}C, PBS$^{+/+}$, pH 7.45, 60 min). Incubations were then quenched and 17-HDHA levels assessed using LM metabololipidomics. Results for a are representative of n = 3 mice. Results for b are mean ± s.e.m. n=3 mice per group. (c) peritoneal macrophages (Mϕ; 1x10^{6} cells/well) from vagotomised mice were incubated with mCD335^{+} ILC3 (7.5x10^{2} cells/well, 6h, 37^{o}C, PBS+/+, 2%FBS). Incubations were quenched and PCTR1 levels determined using lipid mediator profiling. Results are mean±sem n=3 mice per group. *p<0.05 vs Mϕ; #p< 0.05 vs Mϕ plus ILC3. (d) omenta were isolated from naive mice and stained for choline acetyltransferase (red), CD3 (green), F4/80 (cyan) and RoRγt (white) and staining was imaged using confocal microscopy (see methods for details). Magnification x 40. Results are representative of n-4 mice. (e) Mice were subjected to unilateral vagotomy surgery, after 7 days they were administered vehicle, CD335^{+} ILC3 (5x10^{2} cells), DHA (1μM) plus ACh (1nM) or CD335^{+} ILC3 (5x10^{2} cells), DHA (1μM), ACh (1nM) plus Lipoxygenase Inhibitor (10μM; L.I.; see methods for details) 3 h prior to *E. coli* (1x10^{6} CFU/mouse). At the indicated intervals leukocytes were collected and neutrophil counts determined by light microscopy and flow cytometry. (f) Exudate bacterial loads 12h post *E. coli* inoculation. Results are mean ± s.e.m. n= 4 mice per group from two distinct experiments. (g) Human ILC3 expression of 15-lipoxygenase type I (15-LOX) was determined using flow cytometry. Results for a are representative of n = 4 donors. (h) Mice were subjected to unilateral vagotomy surgery, after 7 days they were administered vehicle, ILC3 (1x10^{3} cells), DHA (1μM), plus ACh (1nM) or ILC3 (1x10^{3} cells), DHA (1μM), ACh (1nM) plus Lipoxygenase Inhibitor (10μM; L.I.; see methods for details) 3 h prior to *E. coli* (1x10^{6} CFU/mouse; see methods for details). At the indicated intervals leukocytes were collected and neutrophil

counts determined by light microscopy and flow cytometry. Results are mean ± s.e.m. n= 6 mice per group from two distinct experiments.

Table 1. Vagotomy alters the peritoneal lipid mediator profile.

			Lipid mediators levels (pg/lavage)			
DHA bioactive metabolome	**Q1**	**Q3**	**Sham**	**Day 1**	**Day 3**	**Day 7**
RvD1	375	141	2.5 ± 1.7	5.0 ± 4.7	0.2 ± 0.2	2.0 ± 0.8
RvD2	375	141	3.4 ± 1.9	84.0 ± 23.3	0.4 ± 0.0	1.2 ± 0.1
RvD3	375	147	0.1 ± 0.2	*	*	*
RvD4	375	101	1.3 ± 1.0	5.9 ± 3.6	0.9 ± 0.2	1.4 ± 0.4
RvD5	359	199	16.3 ± 8.4	35.8 ± 8.1	3.4 ± 1.9	7.5 ± 2.0
RvD6	359	101	1.7 ± 1.5	2.9 ± 1.4	0.2 ± 0.1	0.3 ± 0.1
17R-RvD1	375	141	0.5 ± 0.4	5.5 ± 3.8	*	*
17R-RvD3	375	147	0.3 ± 0.3	1.3 ± 0.9	0.1 ± 0.1	0.1 ± 0.1
PD1	359	153	27.5 ± 14.2	45.1 ± 14.2	11.1 ± 3.6	19.4 ± 5.4
17R-PD1	359	153	22.9 ± 12.7	39.5 ± 6.9	10.4 ± 3.5	20.7 ± 6.8
10S,17S-diHDHA	359	153	218.9 ± 136.8	1057.1 ± 232.6	61.8 ± 19.2	170.7 ± 49.7
PCTR1	650	231	15.3 ± 4.5	2.9 ± 1.7	1.1 ± 0.2	2.8 ± 1.3
PCTR2	521	231	12.4 ± 5.9	6.5 ± 5.7	1.2 ± 0.1	3.1 ± 1.2
PCTR3	464	231	9.8 ± 6.2	0.2 ± 0.1	*	0.1 ± 0.1
MaR1	359	221	0.3 ± 0.3	*	0.4 ± 0.1	1.2 ± 0.4
7S,14S-diHDHA	359	221	26.5 ± 16.3	755.4 ± 144.4	10.4 ± 9.4	8.3 ± 1.6
4S,14S-diHDHA	359	101	36.6 ± 31.8	167.3 ± 60.2	1.6 ± 0.6	8.5 ± 2.3
EPA bioactive metabolome						
RvE1	349	195	2.2 ± 0.7	4.9 ± 1.9	*	0.4 ± 0.3
RvE2	333	199	1.3 ± 0.7	7.0 ± 1.7	0.3 ± 0.3	0.6 ± 0.4
RvE3	333	201	1.0 ± 0.8	1.5 ± 0.9	0.1 ± 0.1	0.4 ± 0.1
AA bioactive metabolome						
LXA_4	351	217	0.2 ± 0.1	5.7 ± 1.7	0.1 ± 0.1	0.1 ± 0.1
LXB_4	351	221	2.7 ± 1.4	36.2 ± 13.2	*	0.6 ± 0.2
5S,15S-diHETE	335	235	116.7 ± 67.1	1255.9 ± 362.4	18.2 ± 9.3	42.2 ± 14.2
15R-LXA_4	351	217	3.5 ± 2.4	151.9 ± 64.0	1.6 ± 0.3	3.1 ± 0.6
15R-LXB_4	351	221	4.4 ± 3.0	4.8 ± 1.8	2.2 ± 0.5	2.5 ± 0.6
LTB_4	335	195	25.8 ± 9.8	246.8 ± 128.1	4.9 ± 1.7	13.4 ± 4.2
5S,12S-diHETE	335	195	34.0 ± 25.4	406.7 ± 93.1	1.3 ± 0.7	4.0 ± 2.7
20-OH-LTB_4	351	195	0.1 ± 0.1	0.3 ± 0.2	0.1 ± 0.1	0.1 ± 0.1
LTC_4	626	189	70.2 ± 20.3	12.4 ± 4.0	10.5 ± 3.6	23.2 ± 10.4
LTD_4	497	189	30.3 ± 18.1	22.9 ± 11.9	11.2 ± 3.4	27.7 ± 14.1
LTE_4	440	189	11.1 ± 6.7	0.7 ± 0.3	0.9 ± 0.4	0.8 ± 0.2
PGD_2	351	189	50.3 ± 30.1	230.1 ± 82.4	16.8 ± 4.7	32.3 ± 12.0
PGE_2	351	189	117.9 ± 37.7	194.6 ± 69.8	61.6 ± 22.0	163.2 ± 83.9
$PGF_{2\alpha}$	353	193	33.4 ± 14.4	72.1 ± 12.0	26.2 ± 18.1	30.0 ± 9.9
TxB_2	369	169	95.1 ± 34.0	52.3 ± 31.7	60.8 ± 7.3	101.9 ± 32.8

Mice were subjected to vagotomy or sham procedure, peritoneal lavages were collected at the indicated intervals and LM levels were assessed using LM-metabololipidomics. Results are expressed as pg/lavage; mean ± s.e.m.; n = 3-5 mice per group. $^{\#}$ $p < 0.05$ *vs* Sham, * = below limit, limit ≈ 0.1 pg. With Q1, M-H (parent ion); and Q3, diagnostic ion in the MS-MS (daughter ion).

Robinette, M.L., Fuchs, A., Cortez, V.S., Lee, J.S., Wang, Y., Durum, S.K., Gilfillan, S., Colonna, M., and Immunological Genome, C. (2015). Transcriptional programs define molecular characteristics of innate lymphoid cell classes and subsets. Nat Immunol *16*, 306-317.

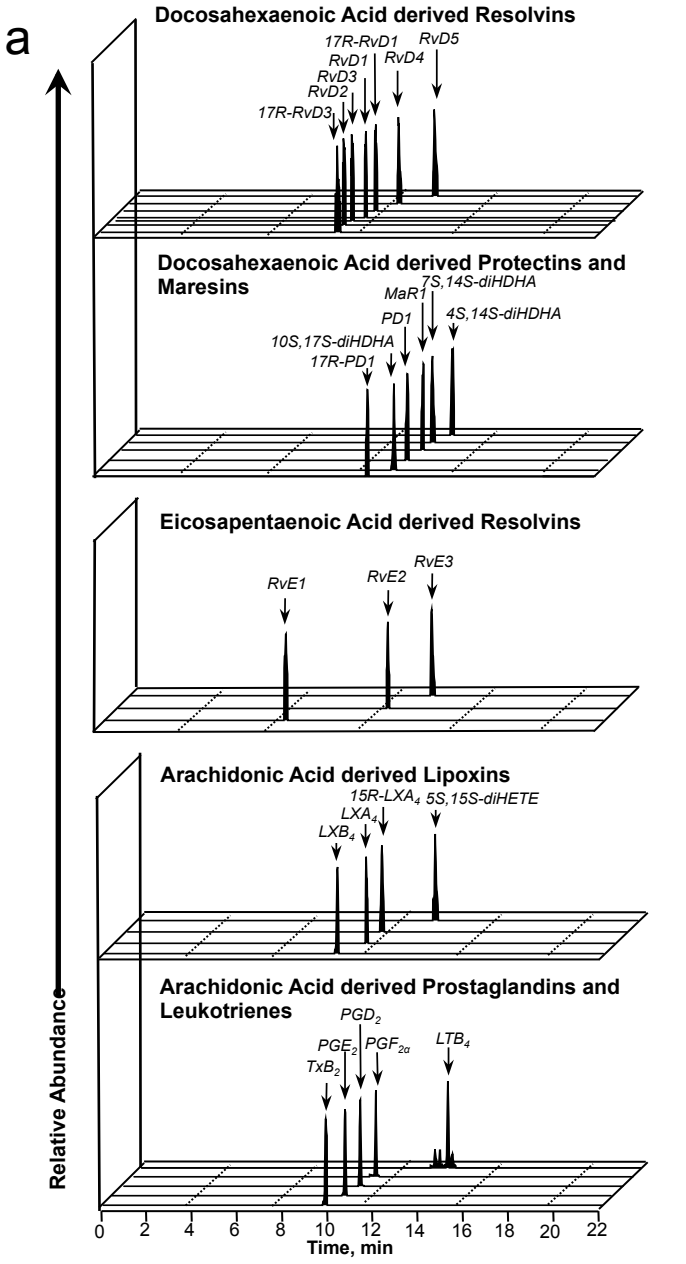
a
Docosahexaenoic Acid derived Resolvins
17R-RvD1
RvD1
RvD3
RvD2
17R-RvD3
RvD5
RvD4
Docosahexaenoic Acid derived Protectins and Maresins
MaR1
7S,14S-diHDHA
PD1
4S,14S-diHDHA
10S,17S-diHDHA
17R-PD1
Eicosapentaenoic Acid derived Resolvins
RvE1
RvE2
RvE3
Arachidonic Acid derived Lipoxins
15R-LXA4
5S,15S-diHETE
LXA4
LXB4
Arachidonic Acid derived Prostaglandins and Leukotrienes
PGD2
PGE2
PGF2α
LTB4
TxB2
Relative Abundance
0 2 4 6 8 10 12 14 16 18 20 22
Time, min

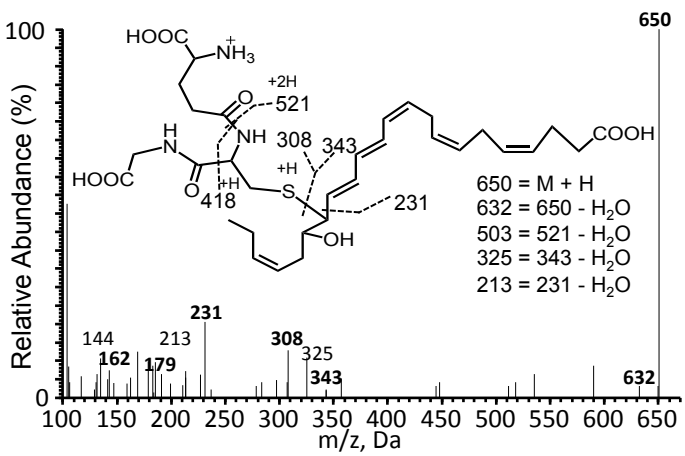
b
100
0
Relative Abundance (%)
650
HOOC
NH3
+2H
521
NH
308
343
COOH
HOOC
+H
418
+H
S
231
OH
650 = M + H
632 = 650 - H2O
503 = 521 - H2O
325 = 343 - H2O
213 = 231 - H2O
231
144
213
308
162
179
325
343
632
100 150 200 250 300 350 400 450 500 550 600 650
m/z, Da

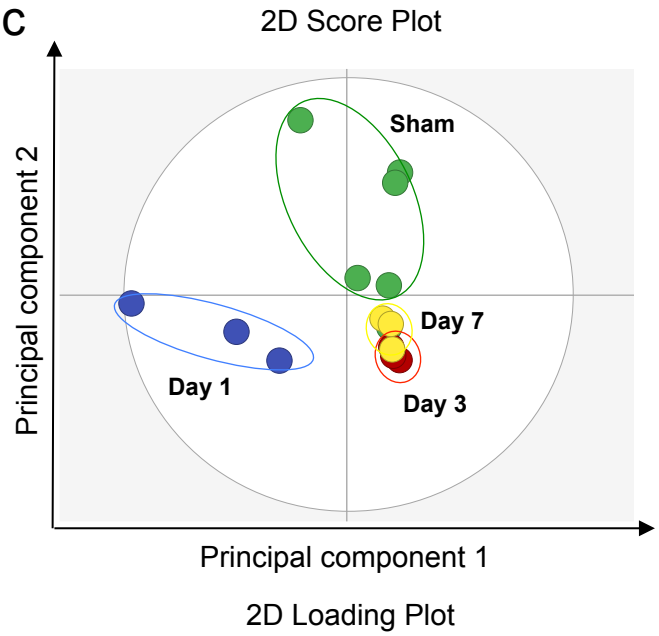
c
2D Score Plot
Sham
Day 7
Day 1
Day 3
Principal component 2
Principal component 1

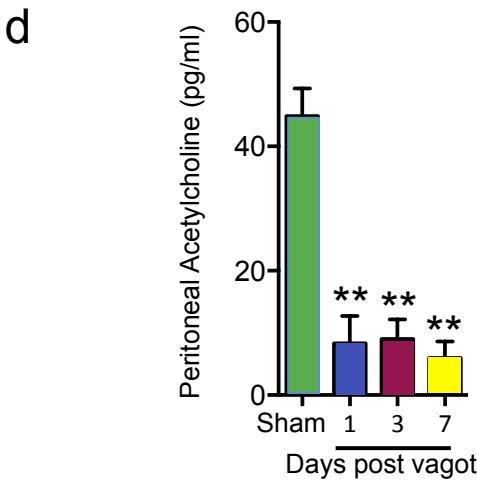
d
Peritoneal Acetylcholine (pg/ml)
60
40
20
0
**
**
**
Sham
1
3
7
Days post vagotomy

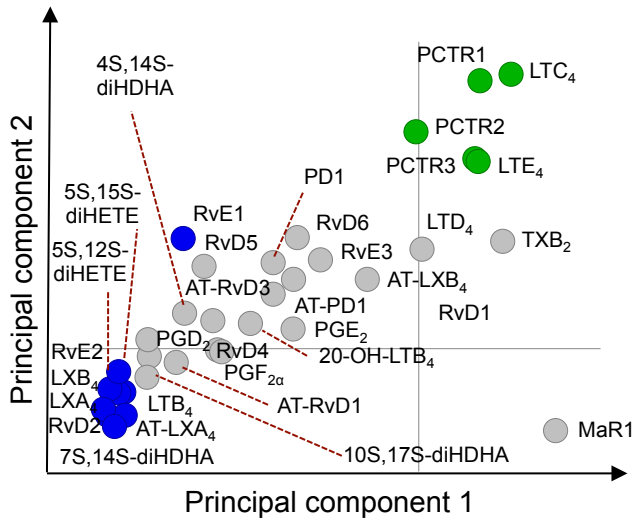
2D Loading Plot
4S,14S-diHDHA
PCTR1
LTC4
PCTR2
PCTR3
LTE4
PD1
5S,15S-diHETE
RvE1
RvD6
LTD4
TXB2
RvD5
5S,12S-diHETE
RvE3
AT-LXB4
AT-RvD3
RvD1
AT-PD1
PGE2
PGD2
RvD4
20-OH-LTB4
RvE2
LXB4
PGF2α
LXA4
LTB4
AT-RvD1
RvD2
AT-LXA4
MaR1
7S,14S-diHDHA
10S,17S-diHDHA
Principal component 2
Principal component 1

Figure 2

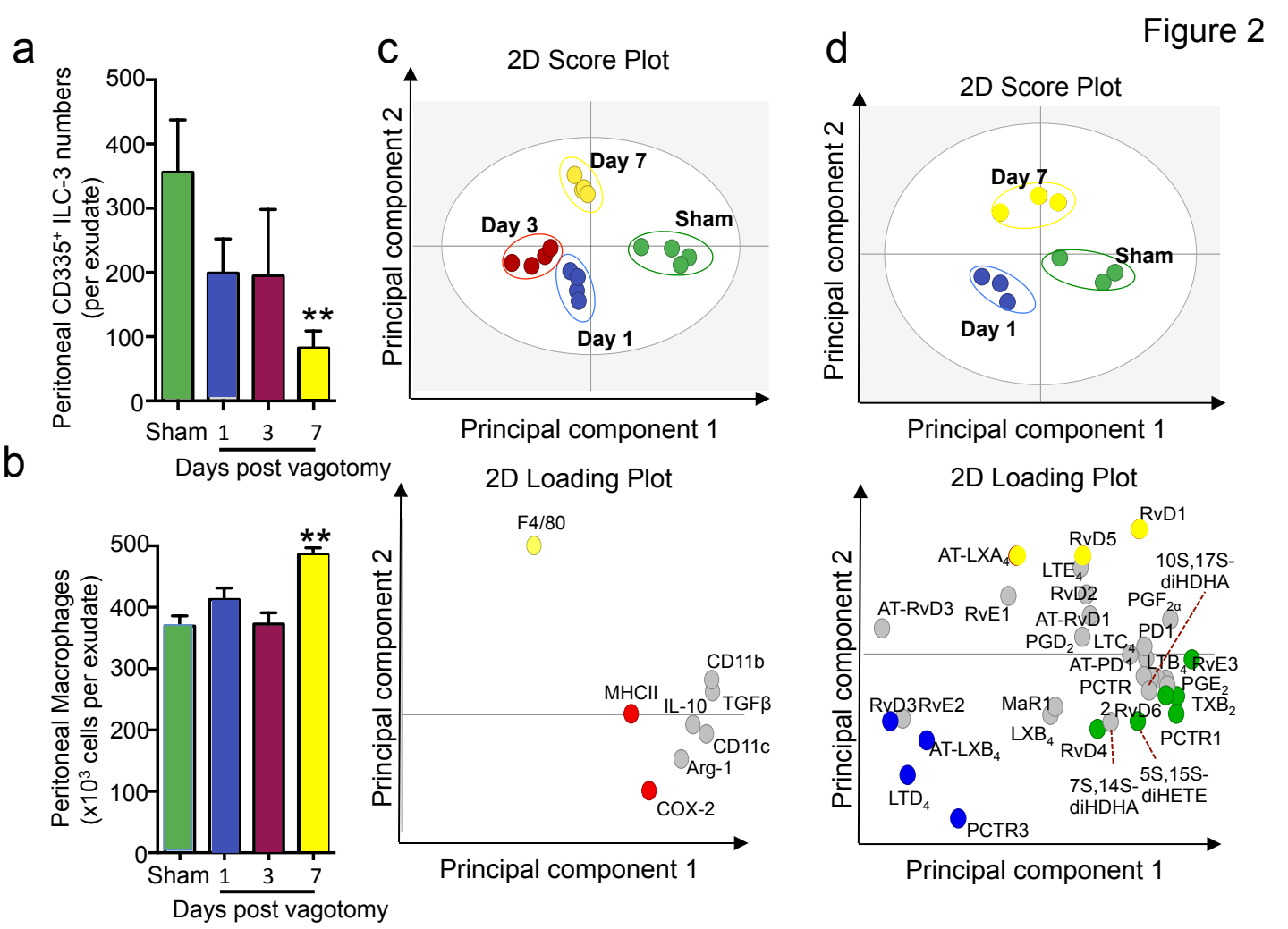
a
Peritoneal CD335+ ILC-3 numbers (per exudate)
500
400
300
200
100
0
**
Sham 1 3 7
Days post vagotomy
b
Peritoneal Macrophages (x10³ cells per exudate)
500
400
300
200
100
0
**
Sham 1 3 7
Days post vagotomy
c
2D Score Plot
Principal component 2
Principal component 1
Day 7
Day 3
Sham
Day 1
2D Loading Plot
Principal component 2
Principal component 1
F4/80
CD11b
MHCII
IL-10
TGFβ
CD11c
Arg-1
COX-2
d
2D Score Plot
Principal component 2
Principal component 1
Day 7
Sham
Day 1
2D Loading Plot
Principal component 2
Principal component 1
RvD1
RvD5
AT-LXA4
LTE4
10S,17S-diHDHA
RvD2
PGF2α
AT-RvD3
RvE1
AT-RvD1
PGD2
LTC4
PD1
AT-PD1
LTB4
RvE3
PCTR
PGE2
RvD3
RvE2
MaR1
2
RvD6
TXB2
LXB4
RvD4
PCTR1
AT-LXB4
5S,15S-diHETE
7S,14S-diHDHA
LTD4
PCTR3

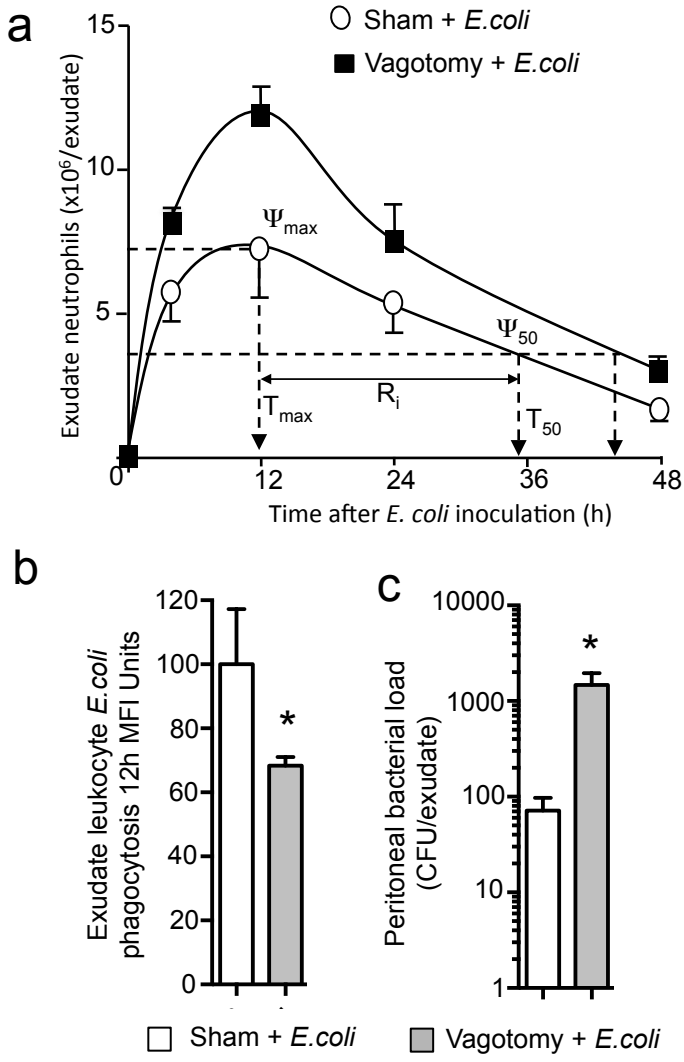
a
Sham + E.coli
Vagotomy + E.coli
Exudate neutrophils (x10⁶/exudate)
15
10
5
0
Ψmax
Ψ50
Ri
Tmax
T50
12
24
36
48
Time after E. coli inoculation (h)
b
Exudate leukocyte E.coli phagocytosis 12h MFI Units
120
100
80
60
40
20
0
*
c
Peritoneal bacterial load (CFU/exudate)
10000
1000
100
10
1
*
Sham + E.coli
Vagotomy + E.coli

Figure 4

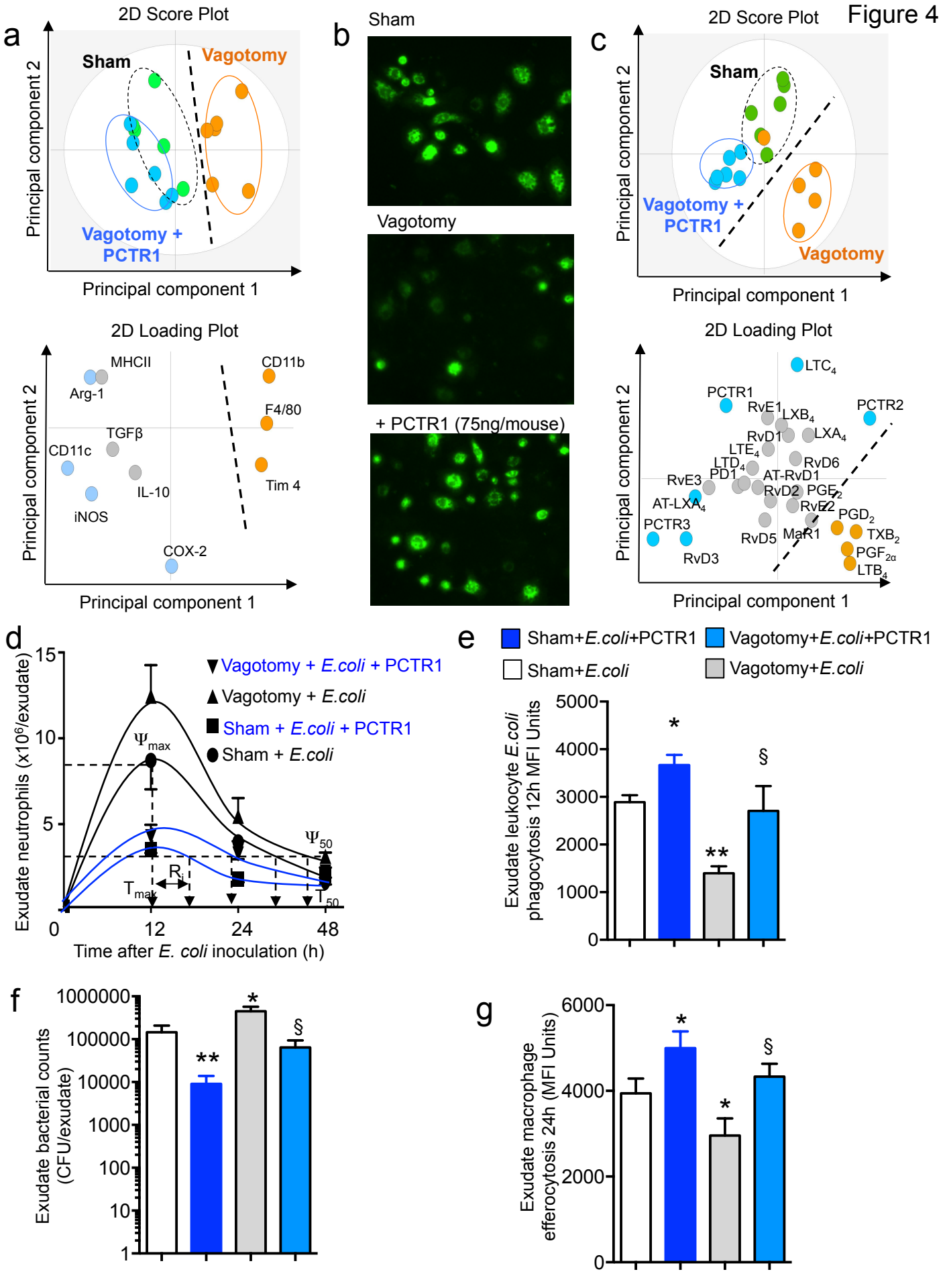
a
2D Score Plot
Sham
Vagotomy
Vagotomy + PCTR1
Principal component 2
Principal component 1
2D Loading Plot
MHCII
CD11b
Arg-1
F4/80
TGFβ
CD11c
IL-10
Tim 4
iNOS
COX-2
b
Sham
Vagotomy
+ PCTR1 (75ng/mouse)
c
2D Score Plot
Sham
Vagotomy + PCTR1
Vagotomy
Principal component 2
Principal component 1
2D Loading Plot
LTC4
PCTR1
RvE1
LXB4
PCTR2
RvD1
LXA4
LTE4
LTD4
RvD6
PD1
AT-RvD1
RvE3
RvD2
PGE2
AT-LXA4
RvE2
PGD2
PCTR3
RvD5
MaR1
TXB2
RvD3
PGF2α
LTB4
Principal component 2
Principal component 1
d
Vagotomy + E.coli + PCTR1
Vagotomy + E.coli
Sham + E.coli + PCTR1
Sham + E.coli
Ψmax
Ψ50
Ri
Tmax
T50
Exudate neutrophils (x10^6/exudate)
Time after E. coli inoculation (h)
e
Sham+E.coli+PCTR1
Vagotomy+E.coli+PCTR1
Sham+E.coli
Vagotomy+E.coli
Exudate leukocyte E.coli phagocytosis 12h MFI Units
f
Exudate bacterial counts (CFU/exudate)
g
Exudate macrophage efferocytosis 24h (MFI Units)

Figure 5

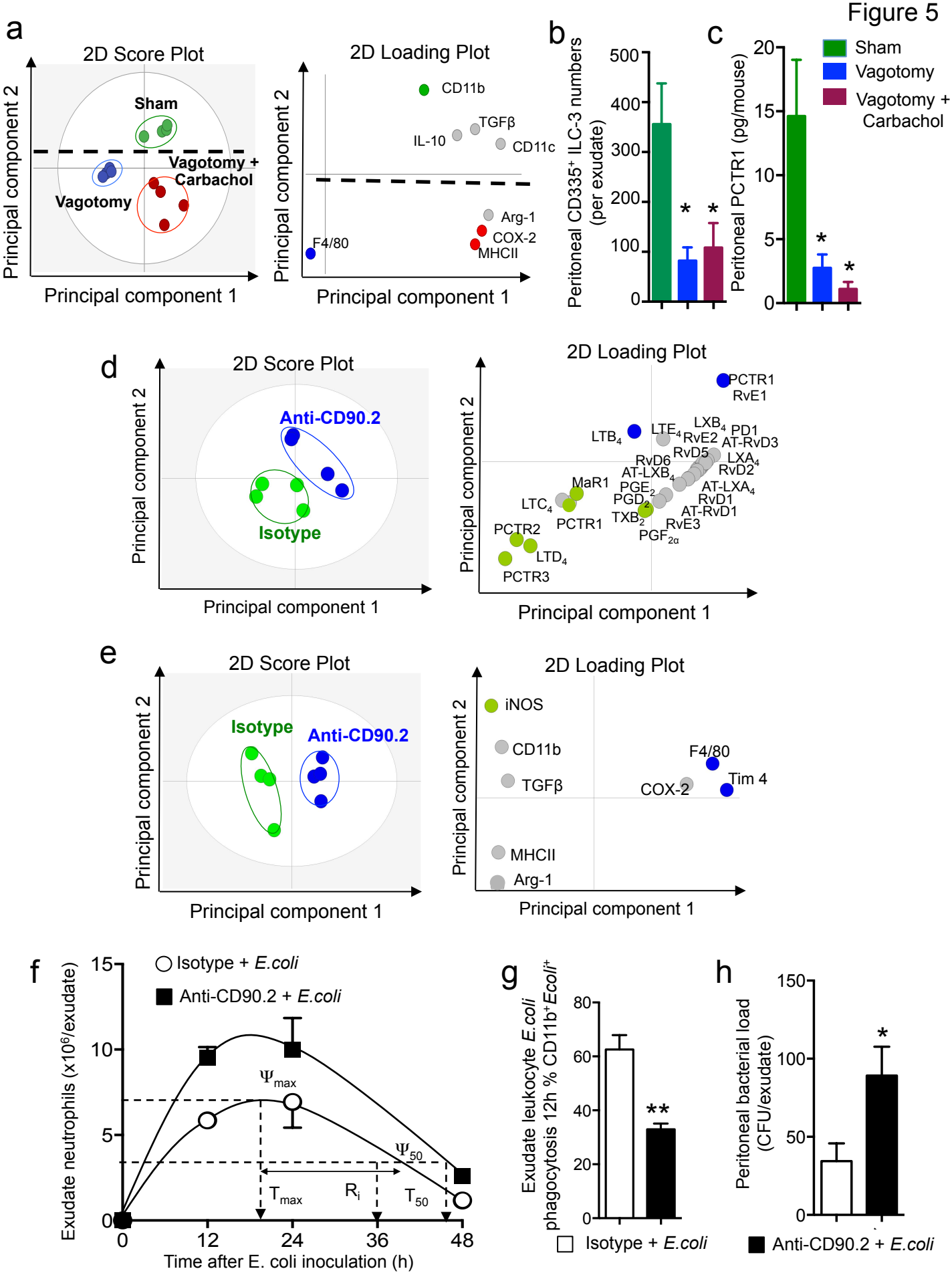
a
2D Score Plot
Sham
Vagotomy + Carbachol
Vagotomy
Principal component 2
Principal component 1
2D Loading Plot
CD11b
TGFβ
IL-10
CD11c
Arg-1
COX-2
MHCII
F4/80
Principal component 2
Principal component 1
b
Peritoneal CD335+ ILC-3 numbers (per exudate)
500
400
300
200
100
0
*
*
c
Peritoneal PCTR1 (pg/mouse)
20
15
10
5
0
*
*
Sham
Vagotomy
Vagotomy + Carbachol
d
2D Score Plot
Anti-CD90.2
Isotype
Principal component 2
Principal component 1
2D Loading Plot
PCTR1
RvE1
LTB4
LTE4
LXB4
PD1
RvE2
AT-RvD3
RvD5
RvD6
LXA4
AT-LXB4
RvD2
MaR1
PGE2
AT-LXA4
LTC4
PGD2
RvD1
PCTR1
TXB2
AT-RvD1
PCTR2
RvE3
PGF2α
LTD4
PCTR3
Principal component 2
Principal component 1
e
2D Score Plot
Isotype
Anti-CD90.2
Principal component 2
Principal component 1
2D Loading Plot
iNOS
CD11b
TGFβ
F4/80
Tim 4
COX-2
MHCII
Arg-1
Principal component 2
Principal component 1
f
Isotype + E.coli
Anti-CD90.2 + E.coli
Exudate neutrophils (x10⁶/exudate)
15
10
5
0
Ψmax
Ψ50
Tmax
Ri
T50
0
12
24
36
48
Time after E. coli inoculation (h)
g
Exudate leukocyte E.coli phagocytosis 12h % CD11b+Ecoli+
80
60
40
20
0
**
Isotype + E.coli
h
Peritoneal bacterial load (CFU/exudate)
150
100
50
0
*
Anti-CD90.2 + E.coli

Figure 6

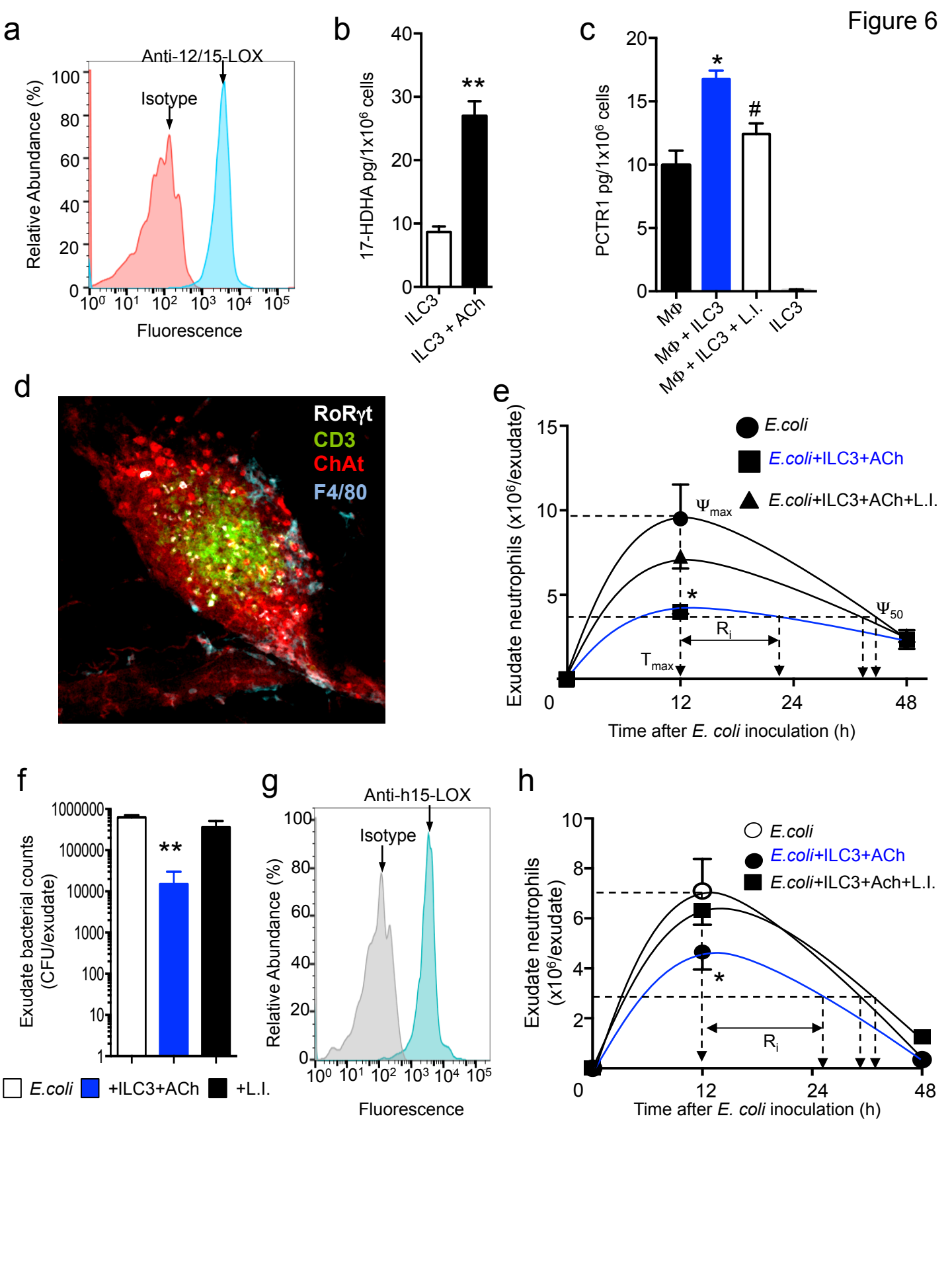
a
Anti-12/15-LOX
Isotype
Relative Abundance (%)
Fluorescence
b
17-HDHA pg/1x10^6 cells
**
ILC3
ILC3 + ACh
c
PCTR1 pg/1x10^6 cells
*
#
MΦ
MΦ + ILC3
MΦ + ILC3 + L.I.
ILC3
d
RoRγt
CD3
ChAt
F4/80
e
Exudate neutrophils (x10^6/exudate)
E.coli
E.coli+ILC3+ACh
E.coli+ILC3+ACh+L.I.
Ψmax
Ψ50
Ri
Tmax
Time after E. coli inoculation (h)
f
Exudate bacterial counts (CFU/exudate)
**
E.coli
+ILC3+ACh
+L.I.
g
Anti-h15-LOX
Isotype
Relative Abundance (%)
Fluorescence
h
Exudate neutrophils (x10^6/exudate)
E.coli
E.coli+ILC3+ACh
E.coli+ILC3+Ach+L.I.
Ri
Time after E. coli inoculation (h)